Journal of Crystal Growth 378 (2013) 466–469

Contents lists available at SciVerse ScienceDirect

Journal of Crystal Growth

journal homepage: www.elsevier.com/locate/jcrysgro

The study of self-assembled ZnO nanorods grown on Si(111) by plasma-assisted molecular beam epitaxy

A.J. Tzou [a], K.F. Chien [a], H.Y. Lai [a], J.T. Ku [a], L. Lee [a], W.C. Fan [a], W.C. Chou [a,b,*]

[a] Department of Electrophysics, National Chiao Tung University, Hsin-Chu 30010, Taiwan
[b] NSC Taiwan Consortium of Emergent Crystalline Materials, Taiwan

ARTICLE INFO

Available online 8 January 2013

Keywords:
A1. Nanostructures
A3. Molecular beam epitaxy
B1. Oxides
B1. Zinc compounds
B2. Semiconducting II–VI materials

ABSTRACT

The growth and optical properties of self-assembled ZnO nanorods grown on Si(111) substrate by plasma-assisted molecular beam epitaxy (PA-MBE) were studied. By controlling the Zn/O flux ratio, the growth of ZnO nanorods on Si(111) substrate without catalyst has been achieved. Scanning electron microscopy (SEM) shows the ZnO nanorods with various density and diameter could be controlled. Photoluminescence (PL) measurements exhibit nice optical properties. The sharp near band edge PL emission with full width at half maximum (FWHM) of about 17 meV indicates that the ZnO nanorods could be used as the high efficient photonic devices.

1. Introduction

ZnO has attracted lots of attention due to its superior electrical, optical and piezoelectric properties for the application in light emitting diodes, solar cells and surface acoustic wave devices etc. [1–4]. Compared with two-dimensional epitaxy layers, ZnO nanorod structure has significantly reduced threading dislocation density [5]. Stark effect can be suppressed by growing quantum well structures on the sidewall of *c*-axis oriented nanorod [6]. Therefore, high quality ZnO nanorod of designed structure is important for the application in photonic devices.

The growth of ZnO nanorod has been achieved by vapor–liquid–solid (VLS) method [7], nanoimprint [8] and catalyst-free metal organic chemical vapor deposition (MOCVD) [9]. However, growth of catalyst-free self-assembled ZnO nanorod by MBE was rarely studied [10]. In this article, the growth of high quality ZnO nanorods on Si(111) substrates without catalyst by PA-MBE was accomplished. The crystal structure properties were studied in more details by transmission electron microscopy (TEM) cross-section images and X-ray reciprocal space mapping (RSM).

2. Experiments

ZnO nanorods were grown on Si(111) substrates by using PA-MBE. Silicon substrates were cleaned by 10% HF to remove the native oxide. Before the growth, the substrate was desorbed at 830 °C until Si(111)−(7 × 7) pattern was observed on reflection high energy electron diffraction (RHEED) screen. The substrate temperature was decreased to 650 °C for the deposition of Zn layer for 10 minutes to prevent the formation of amorphous silicon oxide on the desorbed Si(111) surface. The oxygen plasma of 1.5×10^{-5} Torr was then turned on with the oxygen flow rate of 0.6 sccm and RF plasma power of 250 W. The Zn flux was adjusted from 1.00×10^{-8} to 8.61×10^{-8} Torr to vary the Zn/O flux ratio.

The surface morphology and density were analyzed by JEOL JSM-7001F scanning electron microscope (SEM). A high resolution JEOL ARM-200F TEM was employed to study the crystalline properties. The energy dispersive X-ray spectroscopy (EDS) was carried out during the TEM observation to probe the Zn and Si composition distribution in nanorods. The crystal structure was also analyzed by RSM with synchrotron at beam line BL-17B1 in the National Synchrotron Radiation Research Center (NSRRC), Taiwan. The PL spectra were excited by the 325 nm line of a He–Cd laser and analyzed by using a *i*HR-550 monochromator and LN_2 cooling CCD.

3. Results and discussion

In Fig. 1, the SEM images of ZnO nanorods grown with different Zn/O ratios were shown. The nanorod diameter increases with increasing Zn flux. For Zn flux above 5.86×10^{-8} Torr, ZnO nanorods merged, as shown in Fig. 1(c) and (d). As the Zn flux reaches to 8.61×10^{-8} Torr, the rods poorly aligned with irregular shape. Nanorod density and diameter as functions of Zn flux are schematically shown in Fig. 2.

* Corresponding author at: National Chiao Tung University, Department of Electrophysics, Hsin-Chu 30010, Taiwan.
E-mail addresses: jerrytzou.ep00g@nctu.edu.tw (A.J. Tzou), wuchingchou@mail.nctu.edu.tw (W.C. Chou).

0022-0248/$ - see front matter Crown Copyright © 2013 Published by Elsevier B.V. All rights reserved.
http://dx.doi.org/10.1016/j.jcrysgro.2012.12.137

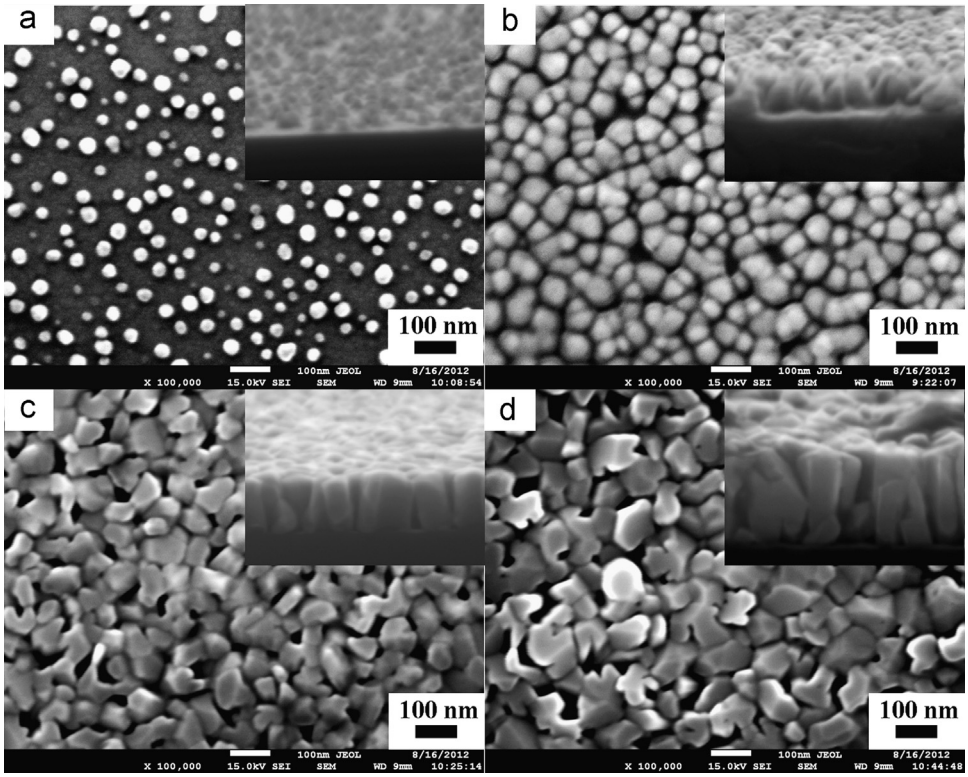

Fig. 1. SEM images of ZnO nanorods grown on Si(111) at various Zn flux: (a) 1.99×10^{-8} Torr, (b) 3.38×10^{-8} Torr, (c) 5.86×10^{-8} Torr, and (d) 8.61×10^{-8} Torr.

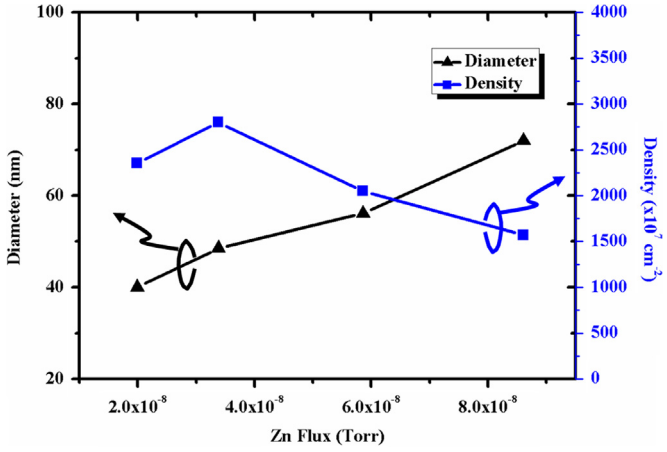

Fig. 2. The density and diameter of ZnO nanorod structure grown at various Zn flux.

The cross-section TEM images of ZnO nanorods grown at Zn flux of 3.38×10^{-8} Torr are shown in Fig. 3(a)–(c). In Fig. 3(a), amorphous SiO_2 was observed between the Si substrate and ZnO nanorods. The existence of amorphous SiO_2 layer implies that the pre-growth of Zn layer has no effect to prevent the formation of silicon dioxide at the initial growth stage. Because of ZnO compounds have weaker bonding than SiO_2 and it is more difficult to crystallize at high growth temperature during the initial stage [11]. It is confirmed by comparing the formation enthalpy of SiO_2 (-910.7 ± 1.0 kJ/mol) and ZnO (-350.46 ± 0.27 kJ/mol) [12]. In Fig. 3(b), there exists a mixed compound layer of about 4 nm between the SiO_2 amorphous layer and ZnO nanorods. As shown in Fig. 3(c), the atomic arrangement of mixed compound layer gradually changes from amorphous to crystalline structure. The constitute elements of this mixed compound layer can be determined by EDS point scan, as shown in Fig. 4. The Cu signal is from the copper holder. The Zn composition gradually increases from the bottom (amorphous SiO_2 side) of mixed compound layer. Whereas, the Si composition decreases when EDS scan moves away from the amorphous SiO_2. This result implies the interdiffusion between Zn and Si [13].

Depth profile RSM of ZnO nanorods was investigated to explore the strain variation in the vertical orientation of crystal structure. In Fig. 5(a), the l axis of reciprocal lattice unit (*r.l.u.*) from 0.02 to 0.16, which is equivalent to scan X-ray from surface to interface, was plotted versus h axis (*r.l.u.*). The intensity shifted slightly in h axis as the scan depth increasing. The h reciprocal lattice unit could be transferred to 2θ degree and schematically shown in Fig. 5(b). In the interfacial region, 2θ diffraction peak situates at 31.66°, which implies tensile strain. When the X-ray beam probed the surface, $l=0.02$, 2θ degree shifted to 31.76°. It implies that the strain is released in the surface region. Thus, this result indicated the ZnO a-axis lattice constant was released from 3.2604 Å to strain free 3.2508 Å, 0.3% strain was released [14].

Fig. 6(a) shows the PL spectrum for ZnO nanorods at 10 K. The strong and sharp near-band edge (NBE) emission peak was observed. The PL emission peak consists of neutral donor bound exciton ($D^\circ X$) at 3.357 eV and free exciton (FX_A) at 3.374 eV [15–16]. In the inset of Fig. 5(a), no deep-level emission peak was observed. The narrow FWHM for the NBE peak, near 17 meV, implies superior quality of the nanorods. Fig. 5(b) shows the temperature-dependent PL measurement. With increasing temperature, the intensity of the $D^\circ X$ peak decreases and the FXA peak dominates along with a simultaneous energy red shift.

4. Conclusions

In summary, growth of self-assembled ZnO nanorods on Si(111) by PA-MBE was achieved. By TEM cross-section image, we can confirm that the well aligned nanorods crystalline structure lies on

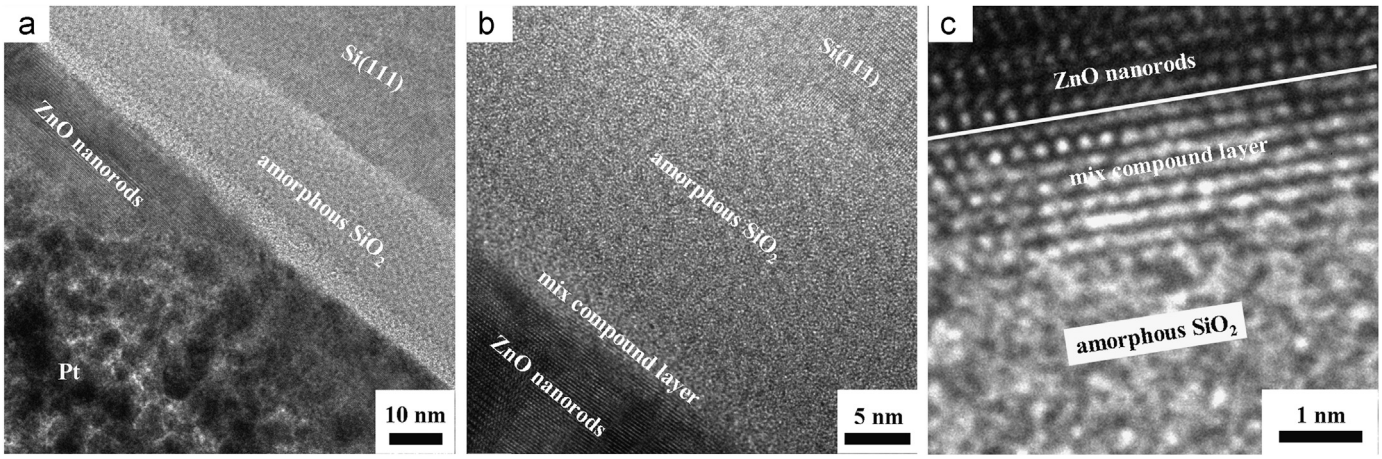

Fig. 3. TEM cross-sectional image of ZnO nanorods grown on Si(111) substrate: (a) low magnification image, (b) and (c) high resolution images of interface and ZnO nanorods, respectively.

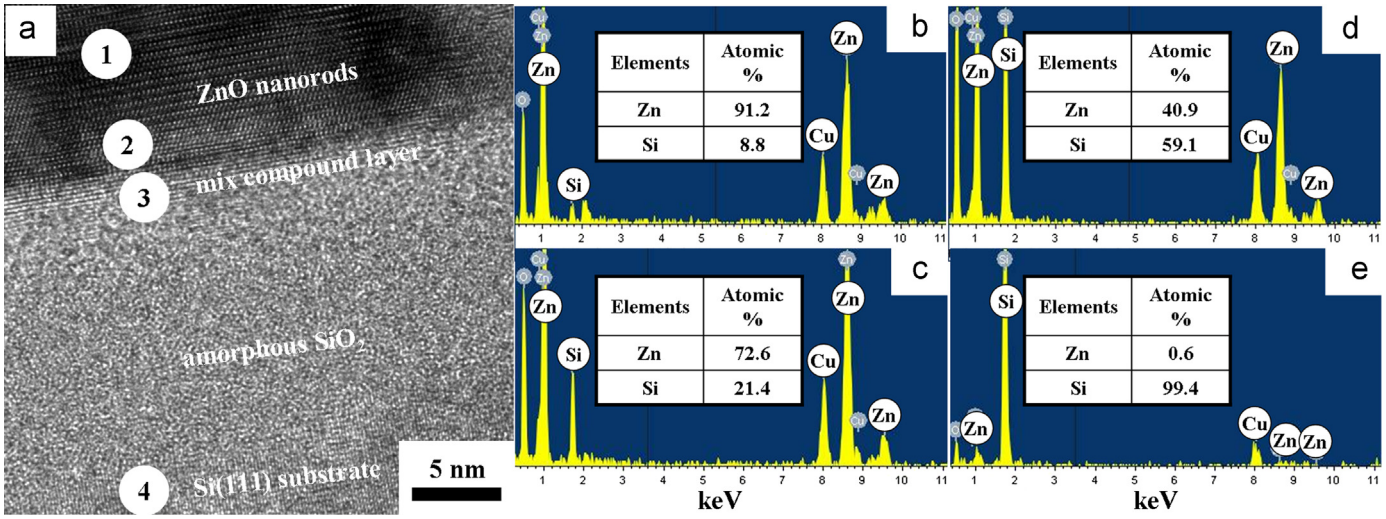

Fig. 4. (a) HRTEM cross-sectional image of ZnO nanorods grown on Si(111) substrate. EDS point scans at the positions of (b) 1, (c) 2, (d) 3, and (e) 4 of Fig. 4(a).

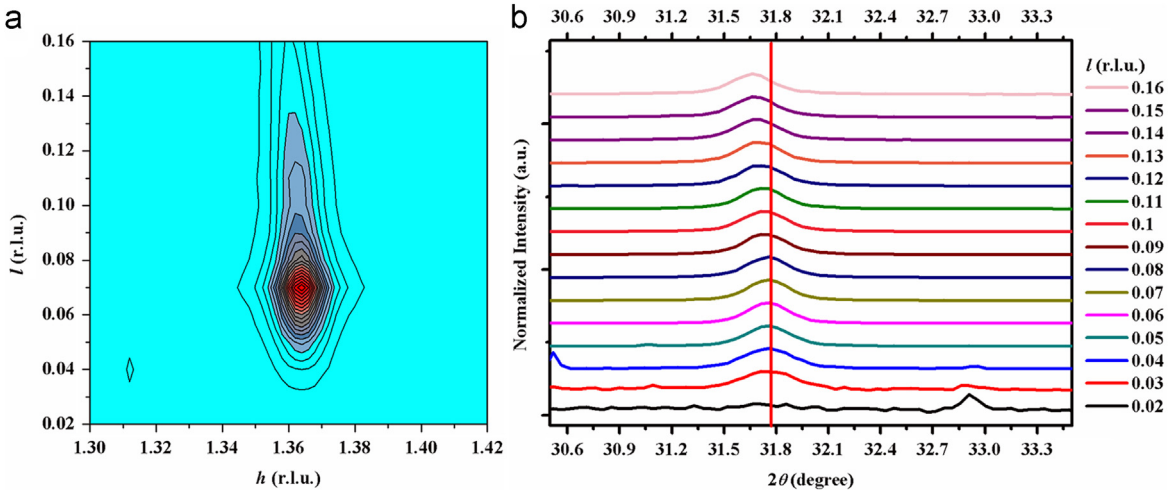

Fig. 5. Depth profile reciprocal space mapping of ZnO nanorods grown on Si(111) substrate. (a) Reciprocal space mapping of l and h axis. (b) 2θ X-ray scan for various l values plot.

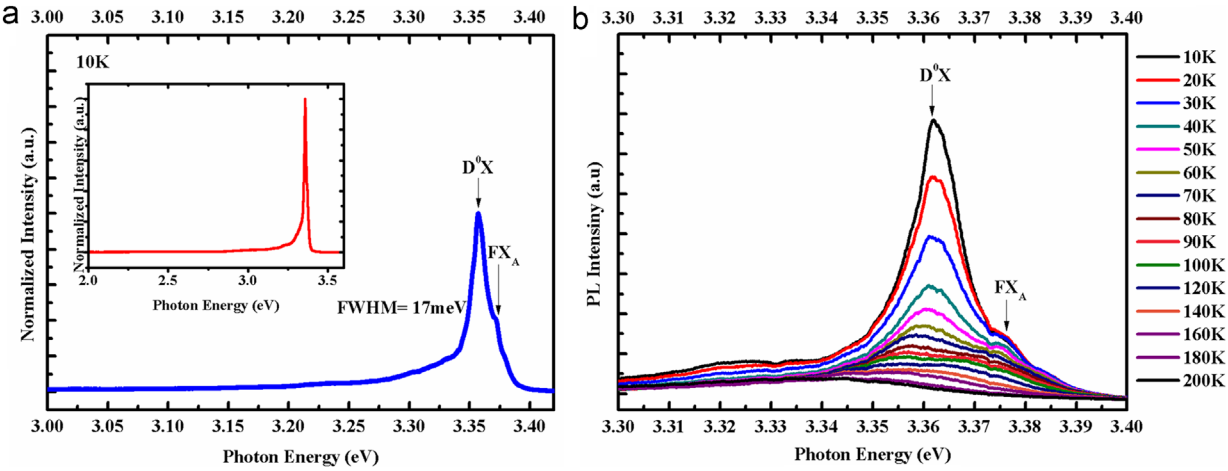

Fig. 6. PL spectra of ZnO nanorods: (a) low temperature PL spectrum, full range PL spectrum is in the inset and (b) temperature-independent PL spectra.

amorphous SiO_2 and a very thin Zn/Si mixed compound layer. The RSM depth profile indicates the strain relaxation of near 0.3% from interface to surface of nanorods. The PL spectra show well optical emission properties. It implies that the nanorods could be used for the further growth of ZnO/ZnMgO nanorod multi-quantum well (MQW) with high emission efficiency.

Acknowledgments

This work was supported by the National Science Council under the Grant number of NSC100-2119-M-009-003.

References

[1] Y.S. Choi, J.W. Kang, D.K. Hwang, S.J. Park, IEEE Transactions on Electron Devices 57 (2010) 26–41.
[2] Z. Liu, X.F. Wang, H. Yang, Y. Duan, Y.P. Zeng, Journal of Semiconductors 31 (2010) 094002.
[3] Q. Zhang, C.S. Dandeneau, X.Y. Zhou, G. Cao, Advanced Materials 21 (2009) 4087–4108.
[4] Q.J. Wang, C. Pflügl, W.F. Andress, D. Ham, F. Capasso, M. Yamanishi, Journal of Vacuum Science and Technology B 26 (6) (2008) 1848–1851.
[5] Y.S. Chen, W.Y. Shiao, T.Y. Tang, W.M. Chang, C.H. Liao, C.H. Lin, K.C. Shen, C.C. Yang, M.C. Hsu, J.H. Yeh, T.C. Hsu, Journal of Applied Physics 106 (2009) 023521.
[6] T. Takeuchi, S. Sota, M. Katsuragawa, M. Komori, H. Takeuchi, H. Amano, Isamu Akasaki, Japanese Journal of Applied Physics Part 2 36 (1997) L382.
[7] N.S. Ramgir, K. Subannajui, Y. Yang, R. Grimm, R. Michiels, Margit Zacharias, Journal of Physical Chemistry C 114 (2010) 10323–10329.
[8] M.H. Jung, H. Lee, Nanoscale Research Letters 6 (2011) 159.
[9] M. Rosina, P. Ferret, P.H. Jouneau, I.C. Robin, F. Levy, G. Feuillet, M. Lafossas, Microelectronics Journal 40 (2009) 242–245.
[10] J.F. Yan, Y.M. Lu, H.W. Liang, Y.C. Liu, B.H. Li, X.W. Fan, J.M. Zhou, Journal of Crystal Growth 280 (2005) 206.
[11] D.C. Kim, J.H. Lee, S.K. Mohanta, H.K. Cho, H. Kim, J.Y. Lee, CrystEngComm 13 (2011) 813–818.
[12] D.R. Lide, 80th Edition,CRC Handbook of Chemistry and Physics, 5, Chemical Rubber, Boca Raton, FL, 2000.
[13] X. Xu, P. Wang, Z. Qi, H. Ming, J. Xu, H. Liu, C. Shi, G. Lu, W. Ge, Journal of Physics: Condensed Matter 15 (2003) L607–L613.
[14] G.K. Bhaumik, A.K. Nath, S. Basu, Materials Science and Engineering B 52 (1998) 25.
[15] B.K. Meyer, J. Sann, D.M. Hofmann, C. Neumann, A. Zeuner, Semiconductor Science and Technology 20 (2005) S62–S66.
[16] A. Teke, Ü. Özgür, S. Dogan, X. Gu, H. Morkoç, B. Nemeth, J. Nause, H.O. Everitt, Physical Review B 70 (2004) 195207.